

Star Formation in the Eagle Nebula

Joana M. Oliveira

*School of Physical and Geographical Sciences, Lennard-Jones Laboratories,
 Keele University, Staffordshire ST5 5BG, UK*

Abstract. M16 (the Eagle Nebula) is a striking star forming region, with a complex morphology of gas and dust sculpted by the massive stars in NGC 6611. Detailed studies of the famous “elephant trunks” dramatically increased our understanding of the massive star feedback into the parent molecular cloud. A rich young stellar population (2–3 Myr) has been identified, from massive O-stars down to substellar masses. Deep into the remnant molecular material, embedded protostars, Herbig-Haro objects and maser sources bear evidence of ongoing star formation in the nebula, possibly triggered by the massive cluster members. M16 is an excellent template for the study of star formation under the hostile environment created by massive O-stars. This review aims at providing an observational overview not only of the young stellar population but also of the gas remnant of the star formation process.

1 Overview

The cluster Messier 16 (M16), in the constellation Serpens Cauda, was first discovered in 1745 by Jean-Philippe Loys de Cheseaux, a Swiss astronomer from Lausanne, who in 1746 presented to the French Academy of Science a list of clusters and nebulae, including M16. On June 3, 1764, Charles Messier independently discovered the cluster, noting its nebulous nature, and gave it the number M16 by which it is now known. It was later included in John Herschel’s catalogue of clusters and nebulae as h2006, and eventually received the designation NGC 6611 when listed in Dreyer’s New General Catalogue. In the popular literature, it is often known as the Eagle Nebula.

The massive stars in the young cluster NGC 6611 (Walker 1961) are responsible for the ionization of the H II region identified as Sh2–49 (Sharpless 1959), Gum 83 (Gum 1955) or RCW 165 (Rodgers, Campbell & Whiteoak 1960) in the optical or W 37 (Westerhout 1958) as observed at radio wavelengths. These stars have been photoevaporating the surrounding parent molecular cloud and sculpting the overdense molecular cores into the famous “elephant trunks” (Fig. 1). First identified by Duncan (1920), these structures were revealed in their full glory in the iconic HST images of Hester et al. (1996); they appear in the optical images as opaque fingers or columns of dense obscuring material projected against the diffuse background nebular emission. Even if not as dense as originally thought (Thompson, Smith & Hester 2002), these columns harbour small protrusions on or near their surface, the EGGs, a fraction of which seem to be associated with embedded Young Stellar Objects (YSOs), signs of a recent episode of star formation (e.g. McCaughrean & Andersen 2002).

NGC 6611 cluster members are distributed over a region of ~ 14 arcmin radius, with a higher concentration in the largely unobscured 4 arcmin radius central area (Belikov et al. 2000; Kharchenko et al. 2005). The cluster contains a large number of

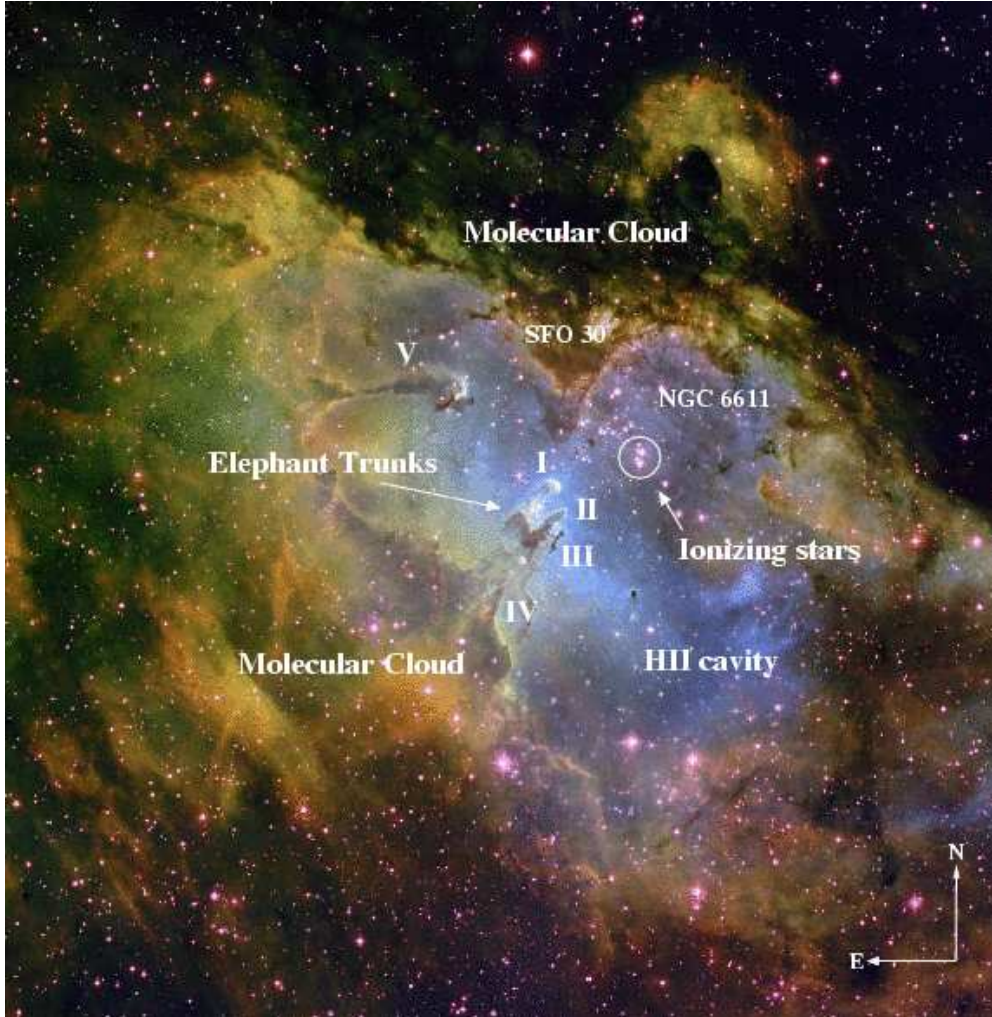


Figure 1. Wide-field image (approximately $40 \text{ arcmin} \times 41 \text{ arcmin}$) of the Eagle Nebula, showing the blister H II region created by the massive stars in NGC 6611. Towards the center of the image the dusty pillars are clearly seen (labelled from I to V). This image was taken with the 0.9 m telescope at the Kitt Peak Observatory with the NOAO Mosaic CCD camera and it combines $H\alpha$ (green), $[\text{O III}]$ (blue) and $[\text{S II}]$ (red) images. Credit: T.A. Rector, B.A. Wolpa and NOAO.

massive stars as well as a large population of pre-main sequence (PMS) stars (Hillenbrand et al. 1993). These optically visible members of NGC 6611, with masses in the range 2 to $85 M_{\odot}$, have an average age of 2–3 Myr (Hillenbrand et al. 1993; Belikov et al. 2000). More recently a rich low-mass PMS population (down to substellar masses) was identified by Oliveira et al. (2005) and Oliveira, Jeffries & van Loon (2008).

The Eagle Nebula is a superb example of the interaction of massive stars with their environment, showcasing both its destructive power and its potential for triggering star formation at the periphery of the remnant molecular cloud.

2 The H II Region and the Molecular Cloud Structure

Besides the study of the stellar population associated with NGC 6611 (Section 4), earlier work on M 16 concentrated mainly on studying the physical properties and kinematics of the H II region. Numerous $H\alpha$ and radio continuum maps of the region as well as spectra of hydrogen recombination emission lines and OH and HI absorption were obtained in the 60's and 70's and the derived properties of the neutral and ionized gas are summarized in Goudis (1976) and references therein: radial and turbulent velocities, densities and electron temperatures are provided in that paper. Many of those early works also computed kinematic distances (Section 3).

Radio spectra were also used to predict the properties of the ionizing stars in NGC 6611 (Goudis 1975). Felli & Churchwell (1970) resolve the ionized gas distribution into 3 distinct continuum peaks, one in the northern obscured region (Section 2.2) and 2 either side of the main elephant trunks. The ionized gas presents complex velocity fields, as shown by the splitting of the optical emission line profiles into multiple velocity components (Goudis & Meaburn 1976; Elliot, Meaburn & Terrett 1978; Mufson et al. 1981, and references therein), related to the interplay of the ionized flows with surrounding neutral material.

More recent observations of radio recombination lines (hydrogen, helium and carbon) and radio continuum in M 16 can be found in Quireza et al. (2006). García-Rojas et al. (2006) have measured the intensity of ~ 250 emission lines in bright regions in the nebula associated with NGC 6611. This allowed them to constrain the physical conditions in the H II region making use of a variety of line intensity and continuum ratios. Hébrard et al. (2000) and García-Rojas et al. (2006) also detected several deuterium Balmer lines and confirm that fluorescence, not recombination, is the most probable hydrogen excitation mechanism.

2.1 The Elephant Trunks

Morphology and Physical Conditions The main elephant trunks in M 16 are three dense structures of gas and dust situated at the southeast “boundary” of the H II region created by the numerous O-stars in NGC 6611. These are normally referred to as columns I, II and III respectively from northeast to southwest. Hester et al. (1996) used the famous HST/WFPC2 images (Fig. 2) to investigate the morphology of the columns and the ionization conditions at the interface between the H II region and the molecular material. They found that both the observed morphology and ionization structure are well understood in terms of photoionization of the remnant molecular material. In very simple terms, the ionizing radiation that reaches the molecular cloud increases the pressure at the cloud interface, driving a photoevaporative flow of ionized material away from the cloud into the (low density) H II region cavity (see Hester & Desch 2005, for a review). Lower density material is quickly blown away, while denser molecular cores, compressed by the associated shock fronts, survive longer. Near-IR images (Sugitani, Tamura & Nakajima 2002; Thompson et al. 2002) reveal that, instead of being dense continuous structures of gas and dust, columns I and II are made of relatively low-density material, capped by much denser cores that effectively shield the columns from the ionizing radiation (Fig. 3). This shielding is thought to be responsible for the finger-like morphology, with tails pointing away from the ionizing sources (e.g. White et al. 1999). To the southeast of the elephant trunks, there is another complex of molecular cloud material (column IV, Fig. 1), near the Herbig-Haro object

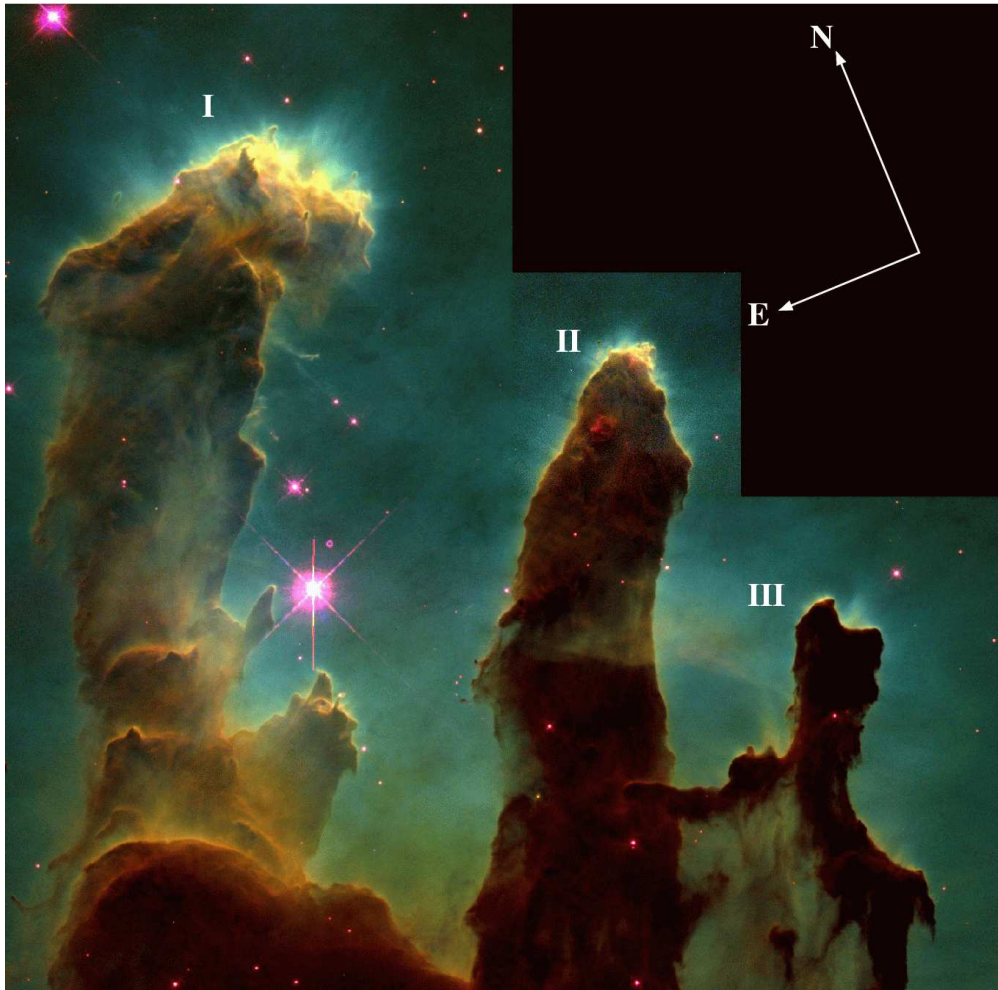


Figure 2. HST WFPC2 colour composite image of a detail of the three central elephant trunks in M 16 (Hester et al. 1996). Columns are labelled I, II and III. Red, green and blue colours show emission from [S II], $H\alpha$ and [O III] respectively. Credit: J. Hester, P. Scowen and STScI.

HH 216 (e.g. Meaburn 1982, Section 7.1). Several authors have used hydrodynamics models to describe the formation and morphology of the Eagle Nebula fingers (e.g. Williams, Ward-Thompson & Whitworth 2001; Miao et al. 2006; Mizuta et al. 2006).

Even at small scales, the structure sculpted by the advancing ionization front is rather complex with numerous dense knots of gas and dust, known as Evaporating Gaseous Globules (EGGs). These have been identified by Hester et al. (1996) at, or near to, the surface of the three columns and have typical sizes of the order of 300–400 AU. It is thought that at least some of these EGGs and the dense column caps are associated with ongoing star formation (see next section).

Observations of the molecular gas in the pillars give further insight into their physical properties. Maps of several CO isotopes probe the velocity field of the molecular

gas in the columns. Pound (1998) and Schuller et al. (2006) found large velocity gradients ($\sim 7.8 \text{ km s}^{-1} \text{ pc}^{-1}$) along the symmetry axis of the pillars with position angles coincident with the direction of the nearby O-stars, supporting the idea that such gradients are produced by the advancing ionization front. White et al. (1999) report on molecular line and continuum emission observations. The dense submillimetre-continuum cores at the top of the columns are constrained to have low dust temperatures ($\sim 10\text{--}20 \text{ K}$), cooler than the surrounding molecular gas ($\gtrsim 60 \text{ K}$). They estimate the masses of these dense caps to be of the order of $10\text{--}60 M_{\odot}$, approximately 55–80% of the mass of each column, as measured from CO observations; the total mass of the three columns is of the order of $\sim 200 M_{\odot}$ (White et al. 1999). Also using CO and millimetre continuum observations, Fukuda, Hanawa & Sugitani (2002) propose a linear sequence of YSOs to starless cores at the head of two of the columns, consistent with star formation activity propagating along them.

Near-IR observations of both molecular and ionized hydrogen emission in the elephant trunks (Allen et al. 1999; Levenson et al. 2000) are useful probes of the physical conditions in the Photo-Dissociation Region (PDR), the interface between the molecular cloud and the H II region where the molecular hydrogen and dust grains are dissociated by the far-UV radiation from the massive stars. Using measured total Br γ fluxes at the head of the columns and assuming that the main ionizing stars are at a projected distance of 2 pc, Allen et al. (1999) find that their combined contribution to the local FUV field is $\sim 16 \text{ erg cm}^{-2} \text{ s}^{-1}$, approximately 10^4 times the ambient interstellar values.

Further evidence of the continuing destruction of the molecular cloud comes from ISOCAM-CVF observations. Mid-IR spectra of the columns reveal emission due to Unidentified Infrared Bands (commonly attributed to Polycyclic Aromatic Hydrocarbons, PAHs) and atomic fine-structure line emission (Urquhart et al. 2003), both good tracers of the PDR conditions. Urquhart et al. (2003) find that UIB emission is contained within the dusty pillars, specially around the tip of column I. From the measured atomic fine-structure line ratios, they estimate a surface ionizing flux of $1\text{--}3 \times 10^{10} \text{ photons cm}^{-2} \text{ s}^{-1}$ (see also White et al. 1999), consistent with the total ionizing flux computed by Allen et al. (1999).

Young Stellar Objects By comparing optical HST and near-IR images, Hester et al. (1996) proposed that the elephants trunks, in particular the EGGs, harbour YSOs and thus are active sites of star formation. White et al. (1999) suggested that cloud cores at the cap of the pillars have temperature and density consistent with those expected in the very early stages of protostellar formation. There is evidence for ongoing star formation in the denser areas of M 16 (maser emission, embedded YSOs) but it is uncertain whether it is being triggered or uncovered by the ionization front from the massive stars (Hester & Desch 2005). Indebetouw et al. (2007) find that the YSO distribution throughout the region supports a picture of distributed low-level star formation, with no strong evidence for triggered star formation in the pillars. Indeed, Ogura et al. (2002) also find no concentration of H α emission stars towards the trunks (section 4.2).

Mid-IR observations (ISO/ISOCAM) revealed only a single embedded source, associated with one of the EGGs, and Pilbratt et al. (1998) suggest that this hints at a rather low level of on-going star formation in the columns. Instrumental limitations, however, made this result inconclusive (Urquhart et al. 2003). Several authors (Sugitani et al. 2002; Thompson et al. 2002; McCaughrean & Andersen 2002) describe embedded YSOs at the tip of two of the columns — these protostars are described in more detail in Section 7. Water maser emission (Healy et al. 2004, Section 6) and



Figure 3. True-colour near-IR image of the elephant trunks in M16 (McCaughrean & Andersen 2002), obtained with ISAAC at the ESO/VLT. *JHK* images are shown respectively as blue, green and red. This image clearly demonstrates that most of the molecular material in the columns sits at their tips. Insets show detail of YSOs embedded in the molecular material, with the numbers referring to the EGGs identified by Hester et al. (1996). The location of the optically visible Herbig-Haro object HH 216 is also indicated (Section 7.1).

Herbig-Haro objects (Andersen et al. 2004, Section 7.1) associated with the columns are further evidence of ongoing star formation.

Walsh & White (1982) identified 8 near-IR sources in the vicinity of the trunks, with 4 of those sources presenting colours consistent with emission from hot circumstellar material. Based on a *JHK* colour-colour diagram, Sugitani et al. (2002) also identify a sample of Class II sources (young stars with circumstellar dust disks) scattered throughout and around the three columns. McCaughrean & Andersen (2002) obtained high-resolution *JHK* images that show the elephant trunks in unprecedented detail (Fig. 3). Of the 73 EGGs they analysed, only $\sim 15\%$ have IR counterparts and are thus associated with young low mass stars. As some EGGs remain opaque even at these wavelengths, this IR-association rate must be considered as a lower limit. Assuming that the observed J and H-band fluxes are photospheric, they derive masses and optical extinction for these IR sources: 7 EGGs are associated with substellar masses while 4 EGGs have masses in the range $0.35\text{--}1\text{ M}_{\odot}$. Linsky et al. (2007) found that none of these 73 EGGs have X-ray counterparts (Section 5). This lack of associated IR and X-ray emission seems to suggest that contrary to what was proposed by Hester et al. (1996), many of the EGGs do not contain embedded YSOs.

2.2 The Bright Rimmed Cloud SFO 30

Bright Rimmed Clouds (BRCs) are dense clumps at the rim of molecular clouds associated with (relatively) old H II regions. Following Sugitani, Fukui & Ogura (1991), BRCs are now commonly referred to as SFOs. SFO 30 is associated with the source IRAS 18159–1346, situated in the optically extincted region to the northeast of the ionizing stars in NGC 6611 (also called the north bay). Morgan et al. (2004) used archival radio, optical and IR images to characterise the physical properties of many BRCs. They compare the gas pressure of the ionized boundary layer and of the interior molecular gas and conclude that SFO 30 (and the majority of their sample) is in approximate pressure equilibrium, and therefore it is likely that photoionization induced shocks are propagating into the interior of the molecular cloud. Based on SCUBA observations, Morgan et al. (2008) found that many SFOs harbour star formation in its early stages and SFO 30 is the most luminous core in their sample ($\sim 7000\text{ L}_{\odot}$).

Hillenbrand et al. (1993) identified a population of embedded sources in near-IR images towards this region. H_2O maser emission has also been detected (Healy, Hester & Claussen 2004; Valdetaro et al. 2005) hinting at ongoing star formation in this area of the molecular cloud. A tentative CS detection and failed ammonia detection have been reported by Anglada et al. (1996). One of the continuum peaks detected by Felli & Churchwell (1970) is also in this region.

2.3 Column V

To the northeast of the main dust pillars, there is another elongated column, with a dense cap and a bright rim, identified as column V or “the spire” (Figs. 2 and 4). Meaburn & Walsh (1986) identified a high-speed ionized knot near its tip, that could be an Herbig-Haro object. Multiple water maser emission components have been detected at the tip of this column (Healy et al. 2004, Section 6) as well as the MSX point source G017.0335+00.7479 (Egan et al. 2003) 5 arcsec south of one of the maser components. The ISOGAL survey has identified a bright YSO candidate J181925.4–134535 at the base of the column (Felli et al. 2002). Recently, Indebetouw et al. (2007), using Spitzer Space Telescope IRAC and MIPS images (Fig. 5), identified the mid-IR counterparts of



Figure 4. Optical composite image of column V in M16, also known as “the spire”. These images were obtained with the instruments ACS and WFC on-board HST. Star formation is occurring in this dusty pillar (Section 7.2). Credit: NASA, ESA, and The Hubble Heritage Team (STScI/AURA).

the maser emission and constrained the properties of the IR source at the base of the column (Section 7.2).

2.4 The H II Region at Mid-IR Wavelengths

Recently, Spitzer images (Fig. 5) challenged once again our understanding of M16. Fig. 5 (top) shows a composite of all IRAC bands (3.6, 4.5, 5.8 and $8\ \mu\text{m}$): the stellar population appears blue, ionized gas green and hot dust and PAHs as red. Fig. 5 (bottom) shows the $24\ \mu\text{m}$ image. These images show that the cavity of the H II region is full of warm dust. It has been suggested, based on the morphology of the $24\ \mu\text{m}$ -emitting region, that a supernova explosion might be responsible for heating the dust.

3 Reddening and Distance Determinations

The determination of the distance to NGC 6611 is complicated by the fact that the extinction towards the stars in the cluster does not follow the standard interstellar extinction law (e.g. Sagar & Joshi 1979). Several authors have studied the extinction properties towards NGC 6611 cluster members (Neckel & Chini 1981; Chini & Kruegel 1983; Thé et al. 1990; Hillenbrand et al. 1993; de Winter et al. 1997; Belikov et al. 1999; Yadav & Sagar 2001; Kumar et al. 2004) and they all agree that not only is the optical extinction (A_V) very patchy but the values of R_V (the ratio of total to selective extinction), estimated on a star by star basis, seem to be larger than the normal interstellar medium value, suggesting the presence of larger dust grains. Indeed, polarimetric observations by Orsatti, Vega & Marraco (2000, 2006) suggest the presence of larger silicate and graphite grains, when compared with the standard interstellar medium. Reported R_V values towards NGC 6611 are in the range 3.5–4.8 (typical value ~ 3.75 , Hillenbrand et al.

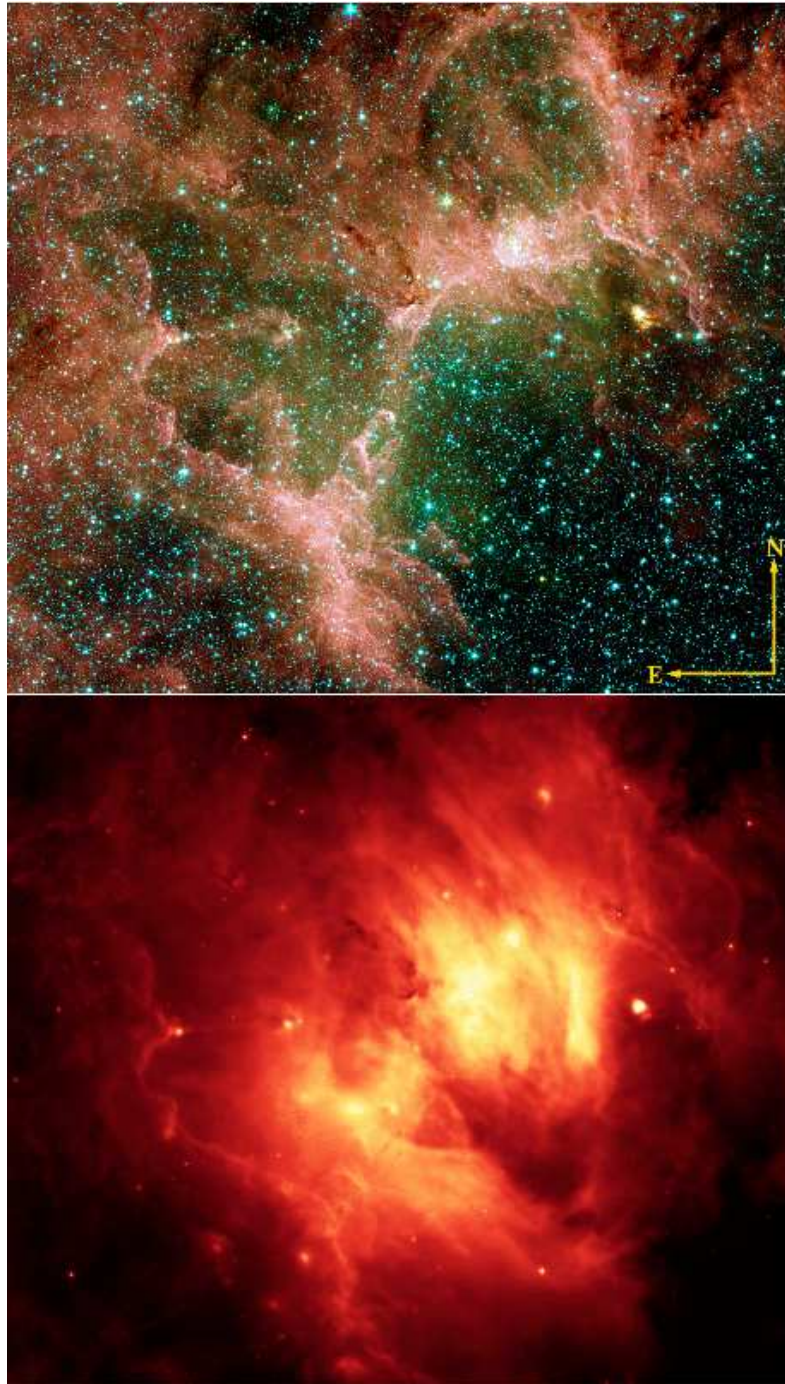


Figure 5. Spitzer images of M16. Top: IRAC composite image, $3.6\,\mu\text{m}$ (blue), $4.5\,\mu\text{m}$ (green), $5.8\,\mu\text{m}$ (orange) and $8\,\mu\text{m}$ (red). Bottom: MIPS $24\,\mu\text{m}$. Credit: NASA/JPL-Caltech/N. Flagey (IAS/SSC) & A. Noriega-Crespo (SSC/Caltech).

Table 1. Distance estimates to NGC 6611.

distance kpc	reference	comment
3.2 ± 0.3	Walker (1961); Sagar & Joshi (1979)	normal extinction law
1.7	Becker (1963)	3-colour photometry
3.4	Mezger & Möglund (1967)	kinematic distance
2.6	Dieter (1967)	kinematic distance
2.2	Miller (1968)	kinematic distance
2.1 ± 0.4	McBreen et al. (1982)	kinematic distance
2.6 ± 0.3	Thé et al. (1990)	anomalous extinction law
2.0 ± 0.1	Hillenbrand et al. (1993)	spectroscopic parallax
2.1 ± 0.1	Belikov et al. (1999)	<i>UBV</i> photometry
1.7	Kharchenko et al. (2005)	photometry
1.8 ± 0.5	Bonatto et al. (2006)	<i>JH</i> photometry
1.8 ± 0.1	Dufton et al. (2006)	spectroscopic parallax
1.75	Guarcello et al. (2007)	<i>VI</i> photometry

1993) while $E(B - V)$ values vary between 0.5–1.1 mag. Typical $E(B - V)$ towards the cluster core is of the order of 0.75 mag (Belikov et al. 1999; Dufton et al. 2006).

Distance determinations to NGC 6611 are summarised in Table 1. Walker (1961) first estimated the distance to NGC 6611 to be 3.2 ± 0.3 kpc, a value also adopted by Sagar & Joshi (1979). Early kinematic distances were in the range 2.2–3.4 kpc (Dieter 1967; Mezger & Möglund 1967; Miller 1968). However, the kinematic distance obtained by McBreen, Fazio & Jaffe (1982) places the cluster considerably closer at 2.1 ± 0.4 kpc. Belikov et al. (1999) estimated the distance by making use of all photometry then available, arriving at a value of 2.14 ± 0.1 kpc. More recent determinations favour an even smaller distance. Dufton et al. (2006) found a distance of 1.8 ± 0.1 kpc, based on spectroscopic parallaxes for 24 massive cluster members. Recent determinations using the main-sequence turnoff (Bonatto, Santos & Bica 2006; Guarcello et al. 2007) are consistent with this latest parallax determination.

4 The Stellar Content of NGC 6611

4.1 High- and Intermediate-mass Population: Cluster Age and IMF

Walker (1961) reported that the intrinsic $V/(B - V)$ colour-magnitude diagram of NGC 6611 consists of a Main Sequence (MS), spectral types O5 to B5, with a population of stars lying above it; he estimated an age of 1.8 Myr for this population. Several photometric studies of the high-mass population have been carried out since, mainly to complete the census of massive stars in the region and to constrain the anomalous reddening law and distance (e.g. Hoag et al. 1961; Hiltner & Morgan 1969; Sagar & Joshi 1979; Thé et al. 1990; Chini & Wargau 1990; Chini, Krügel & Wargau 1992). Proper motion studies have been performed by various authors (van Schewick 1962; Kamp 1974; Tucholke, Geffert & Thé 1986; Hillenbrand et al. 1993; Kharchenko & Schilbach 1995; Belikov et al. 1999; Baumgardt, Dettbarn & Wielen 2000; Loktin & Beshenov 2003). The most recent determination by Kharchenko et al. (2005) lists $\text{pm}_{\text{ra}} = 1.60 \pm 0.33 \text{ mas yr}^{-1}$ and $\text{pm}_{\delta} = -0.35 \pm 0.48 \text{ mas yr}^{-1}$.



Figure 6. ESO Imaging Survey (EIS) optical image of the Eagle Nebula ($\sim 15 \text{ arcmin} \times 11 \text{ arcmin}$ across) with the O stars in NGC 6611 identified (see Table 2). W 205 (O3–O5 V) is shown in red. Observations were carried out using the MPG/ESO 2.2 m Telescope and the ESO NTT at the La Silla Observatory.

The most massive star in NGC 6611 is W 205 or HD 168076, with a mass of $75\text{--}80 M_{\odot}$ (Hillenbrand et al. 1993; Massey et al. 1995; Belikov et al. 2000) and spectral type O3–O5 V (Hillenbrand et al. 1993; Evans et al. 2005). This star was identified early on as the main ionizing source in the Eagle Nebula (Gum 1955; Sharpless 1959; Walker 1961; Gebel 1968; Georgelin & Georgelin 1970; Johnson 1973), accounting for about half the ionizing radiation in the Eagle Nebula (Hester et al. 1996). Massive cluster members seem to have abundances consistent with early-type field stars (Brown et al. 1986; Daflon, Cunha & Butler 2004) and no chemically peculiar stars had until recently been found in the cluster (Pauzen et al. 2002, but see next section). Several studies (e.g. Bosch et al. 1999; Evans et al. 2005) show that members' radial velocities are in agreement with the radial velocity of the ionized gas in the region ($\sim 15 \text{ km s}^{-1}$, Georgelin & Georgelin 1970). Duchêne et al. (2001) conducted an adaptive optics survey of 96 stars in NGC 6611, searching for visual binaries. They found a high frequency of massive binaries ($18 \pm 6\%$) and a lack of mass dependence in the binary properties. In NGC 6611, the binary properties seem to be more consistent with a canonical accretion formation mechanism for OB stars (Beech & Mitalas 1994), rather than the merger mechanism (Bonnell, Bate & Zinnecker 1998). A compilation of the O and B stars (spectral types earlier than B3) in and towards M 16 is provided in Table 2 and the positions of the O stars are shown in Fig. 6.

Table 2.: Massive stars towards NGC 6611. Identifications are from Walker (1961) and Kamp (1974). Positions (J2000) and K magnitudes are from 2MASS (Cutri et al. 2003); spectral types, V magnitudes and $B - V$ colours are from Evans et al. (2005) and Hillenbrand et al. (1993). Membership probabilities (p), computed using positions and proper motions, are from Belikov et al. (1999). Additional references are 1: Kumar et al. (2004); 2: Bosch et al. (1999); 3: Orsatti et al. (2000, 2006); 4: Duchêne et al. (2001); 5: Evans et al. (2005); 6: Alecian et al. (2008).

ID	RA ($^h m s$)	DEC ($^d m s$)	V	B-V	K	SpT	p (%)	other identifications	comments
W412	18:18:58.7	-13:59:28	8.18	0.34	7.39	B0 III	34	HD168183, BD-14°4991	spectroscopic binary ²
W205	18:18:36.4	-13:48:03	8.18	0.43	6.57	O4 V((f+))	41	HD168076, BD-13°4926	visual binary ⁴
W197	18:18:36.1	-13:47:36	8.73	0.45	7.28	O6-7V((f))+B0	46	HD168075, BD-13°4925	spectroscopic binary ²
W401	18:18:56.2	-13:48:31	8.90	0.04	7.58	O8.5 V	46	HD168137, BD-13°4932	intrinsic polarisation ³
-	18:20:34.1	-13:57:16	9.13	0.44	8.02	O8 III	-	HD168504, BD-14°5005	intrinsic polarisation ³
W367	18:18:52.7	-13:49:43	9.39	0.24	8.76	O9.7 IIIp	76	BD-13°4930	
W468	18:19:05.6	-13:54:50	9.40	0.28	8.61	B0.5 V + B1:	47	BD-13°4934	mid-IR excess ¹ ; spectroscopic binary ⁵
W246	18:18:40.1	-13:45:18	9.46	0.82	6.70	O7 II(f)	88	BD-13°4927	intrinsic polarisation ³
W503	18:19:11.1	-13:56:43	9.75	0.49	8.10	B1: e	40	BD-13°4936	H AeBe ¹
W314	18:18:45.9	-13:46:31	9.85	0.58	7.94	O9 V	98	BD-13°4929	suspected spectroscopic binary ^{2,5}
W150	18:18:30.0	-13:49:58	9.85	0.48	8.36	B0.5 V	86	BD-13°4921	intrinsic polarisation ³
W556	18:17:51.0	-13:50:56	9.99	1.19	6.26	B2.5I	40	BD-13°4912	
W125	18:18:26.2	-13:50:05	10.01	0.47	8.60	B1 V + ?	79	BD-13°4920	
W175	18:18:32.7	-13:45:12	10.09	0.84	7.00	O5 V((f+))+ late O	95	BD-13°4923	visual binary ² ; intrinsic polarisation ³
W280	18:18:42.8	-13:46:51	10.12	0.43	8.76	O9.5 Vn	98	BD-13°4928	
W166	18:18:32.2	-13:48:48	10.37	0.57	8.60	O9 V	95		intrinsic polarisation ³
K601	18:19:20.0	-13:54:21	10.68	0.36	9.40	B1.5 V	43	BD-13°4937	H AeBe star; strong magnetic field ⁶
W469	18:19:04.9	-13:48:20	10.69	0.40	9.31	B0.5 Vn	70	BD-13°4933	H AeBe or classical Be ¹ ; intrinsic polarisation ³
W254	18:18:40.8	-13:46:52	10.80	0.47	9.28	B1 V	99		visual binary ⁴
W483	18:19:06.5	-13:43:30	10.99	0.41	9.61	B3 V	72	BD-13°4935	classical Be ¹
W223	18:18:37.9	-13:46:35	11.20	0.59	9.19	B1 V	89		visual binary ⁴
W351	18:18:50.8	-13:48:13	11.26	0.45	9.67	B1 V	-		
W161	18:18:40.0	-13:43:08	11.29	1.05	7.45	O8.5 V	70		mid-IR excess ¹ ; intrinsic polarisation ³
W536	18:19:18.5	-13:55:40	11.46	0.22	10.26	B1.5 V + ?	39		spectroscopic binary ⁵

Table 2.: Massive stars in NGC 6611 (continuation).

ID	RA(^h ^m ^s)	DEC(^d ^m ^s)	V	B-V	K	SpT	p (%)	other identifications	comments
W239	18:18:40.0	−13:54:33	11.48	0.36	10.16	B1.5 V	67		
W210	18:18:37.0	−13:47:53	11.50	0.54	9.99	B1 V	92		
W259	18:18:41.0	−13:45:30	11.56	0.73	9.19	B0.5 V	87		intrinsic polarisation ³
W343	18:18:49.3	−13:46:51	11.72	0.85	8.90	B1V	83		
W296	18:18:44.7	−13:47:56	11.81	0.49	10.10	B1.5 V	95		
W584	18:18:23.6	−13:36:28	12.02	1.05	8.58	O9 V	47		
W207	18:18:36.7	−13:47:33	12.07	0.53	10.17	B1V	89		
W290	18:18:44.9	−13:56:22	12.12	0.46	10.89	B2.5 V	52		
W275	18:18:42.2	−13:46:52	12.12	0.46	10.53	B1.5V	0		visual binary ⁴ ; intrinsic polarisation ³
W301	18:18:45.0	−13:46:25	12.19	0.58	10.30	B2 V	92		
W289	18:18:44.1	−13:48:56	12.60	0.52	10.90	B3 V	95		
W444	18:19:00.4	−13:42:41	12.65	0.92	9.74	B1.5 V	70		
W300	18:18:45.0	−13:47:47	12.69	0.52	10.58	B1.5V	96		
W231	18:18:38.5	−13:45:56	12.71	0.75	10.06	B1V	78		
W311	18:18:45.6	−13:47:53	12.78	0.55	10.77	B3 V	—		visual binary ⁴ ; intrinsic polarisation ³
W227	18:18:38.4	−13:47:09	12.83	0.62	10.60	B2 V	89		visual binary ⁴
W472	18:19:04.7	−13:44:44	12.85	0.53	11.40	B3 V + ?	12		spectroscopic binary ⁵
W409	18:18:57.4	−13:52:12	12.89	0.41	9.91	B2.5 V	66		intrinsic polarisation ³
W297	18:18:44.5	−13:45:48	12.89	0.67	10.41	B2 Vn	10		visual binary ⁴ ; intrinsic polarisation ³
W25	18:18:09.3	−13:46:54	12.93	0.98	9.49	B0.5V	50		visual binary ⁴ ; intrinsic polarisation ³
W267	18:18:41.7	−13:46:44	13.11	0.52	11.37	B3 V	87		visual binary ⁴
W222	18:18:37.5	−13:43:39	13.08	1.35	8.20	O7 V((f))	88		
W188	18:18:33.7	−13:40:58	13.13	1.34	8.78	B0V	68		visual binary ⁴
W541	18:19:19.1	−13:43:52	13.21	0.64	11.19	B1-3 V	56		
W251	18:18:40.4	−13:46:16	13.34	0.69	—	B2V	0		
W371	18:18:53.0	−13:46:45	13.44	0.65	11.16	B0.5V	72		
W305	18:18:45.0	−13:45:25	13.51	1.07	9.80	B1	84		
W228	18:18:38.1	−13:44:25	13.51	0.93	10.08	B2V	86		
W80	18:18:18.2	−13:41:59	13.82	1.64	9.30	B2V	24		
W269	18:18:41.6	−13:42:47	13.98	0.93	10.65	B1.5V	26		

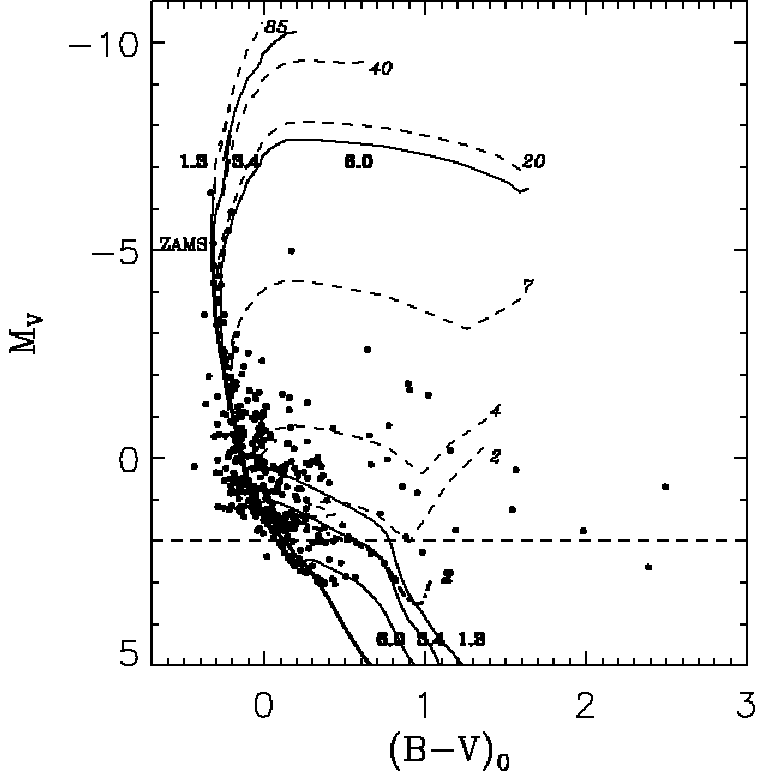


Figure 7. Colour-magnitude diagram of the NGC 6611 cluster members reproduced from Belikov et al. (2000). The ZAMS (Schmidt-Kaler 1982) is shown by a thick line. Thin lines (with bold age labels) are PMS isochrones (1.3, 3.4 and 6 Myr, Palla & Stahler 1993), while the dotted-dashed line at the bottom of the plot is the corresponding PMS track for $2 M_{\odot}$. Post-MS evolutionary tracks (Schaller et al. 1992) are also plotted (dashed lines, with italic mass labels). The PMS population can clearly be seen in this diagram.

Only in the last decade real progress was possible in the study of the cluster PMS. There is a significant population of intermediate-mass stars ($2-8 M_{\odot}$) that sit well above the Zero-Age Main-Sequence (ZAMS) in the Hertzsprung-Russell diagram (Hillenbrand et al. 1993; Belikov et al. 2000, see also the colour-magnitude diagram in Fig. 7). The slope of the Initial Mass Function (IMF; $\Gamma = d \log \xi(\log m) / d \log m$, Scalo 1986) in NGC 6611 is broadly consistent (down to $2 M_{\odot}$) with what is found in other Galactic high-mass star forming regions (Massey et al. 1995), with estimates of Γ in the range -1.5 to -0.7 (Pandey, Mahra & Sagar 1992; Hillenbrand et al. 1993; Massey, Johnson & DeGioia-Eastwood 1995; Belikov et al. 2000; Dufton et al. 2006). Recently, Bonatto et al. (2006) analysed the population of NGC 6611 down to $5 M_{\odot}$ and found that the mass function in the cluster core ($R_{\text{core}} \sim 0.7 \pm 0.1 \text{ pc}^1$) is relatively flat with a slope $\Gamma = -0.62$, while in the halo (to an outer radius of $R_{\text{lim}} \sim 6.5 \pm 0.5 \text{ pc}$) it steepens to a slope of $\Gamma = -1.52$; the overall IMF is similar to a Salpeter IMF with a

¹Guarcello et al. (2007) estimate the cluster core radius to be twice this value, $1.4 \pm 0.08 \text{ pc}$.

slope of $\Gamma = -1.45$. They propose that this spatial variation of the IMF slope may be a consequence of mass segregation in the cluster. This steeper IMF is also consistent with a slope of $\Gamma = -1.5$ as determined by Dufton et al. (2006). The lower-mass IMF is described in Section 4.3.

Considering only the known cluster members more massive than $5 M_{\odot}$, the lower-limit to the observed mass of the cluster is $(1.6 \pm 0.3) \times 10^3 M_{\odot}$ (Bonatto et al. 2006). Assuming that the stars in the mass range $6 - 12 M_{\odot}$ constitute 5.5% of the total mass of the complete population of stars spanning the range $0.1 - 100 M_{\odot}$, Wolff et al. (2007) estimate the total cluster mass to be $\sim 25 \times 10^3 M_{\odot}$ with a density $28.5 M_{\odot} \text{ pc}^{-3}$ (see also Weidner & Kroupa 2006).

The typical age of the NGC 6611 population is of the order of 2–3 Myr but a considerable age spread ($< 1 - 6$ Myr) seems to be present (Hillenbrand et al. 1993; de Winter et al. 1997; Belikov et al. 2000; Dufton et al. 2006). Bonatto et al. (2006) favour a younger age of 1.3 ± 0.3 Myr.

Belikov et al. (1999) compiled most of the then available astrometry and photometry on NGC 6611. From their catalogue of over 2000 objects (available on-line via CDS), Belikov et al. (2000) use astrometric, photometric and proper motion criteria to select 376 probable cluster members (Fig. 7) with masses down to $2 M_{\odot}$.

4.2 H α Emission Stars

Optical photometry and proper motion methods have been commonly used to identify members of NGC 6611 (see previous section). Another classical way to search for young stars in star forming regions are H α emission surveys. Both Herbig AeBe (HAeBe) and Classical T Tauri stars (CTTS) show Balmer line emission, in particular in H α . However, not all young intermediate- and low-mass young stars show emission at all times. It is thought that strong and broad H α emission in young stellar objects originates from the interaction of the star with its circumstellar disk, while weak H α emission originates solely from activity in the stellar chromosphere in young stellar objects without a disk (e.g. White & Basri 2003). Furthermore H α emission is known to be intrinsically variable (e.g. Guenther & Emerson 1997). Taking these considerations into account, H α emission surveys do not detect all low- and intermediate-mass stars in a star forming region; however, particularly in such young clusters like NGC 6611, they are a useful tool to probe the young stellar population.

In bright H II regions like the Eagle Nebula, contamination by the very strong background H α emission is a problem for slit and fibre spectroscopy. As a result, a few HAeBe candidates were identified by Hillenbrand et al. (1993) and de Winter et al. (1997) (2 and 4 objects respectively), but only four of these were confirmed with slitless grism spectroscopy by Herbig & Dahm (2001). Ogura, Sugitani & Pickles (2002) performed a similar survey covering a much larger area, including SFO 30 and much of the elephant trunks. They identified 82 H α emission objects, likely HAeBe and CTTS candidates, distributed throughout the observed area, with no hint of concentration towards the remnant molecular cloud — positions and measurements for these objects are available online via CDS. Kumar et al. (2004) have identified 4 HAeBe candidates based on spectral properties and/or mid-IR excesses. For the HAeBe fast rotator K 601 (or W 601), Alecian et al. (2008) report the detection of a strong magnetic field and the presence of chemical peculiarities in its atmosphere.

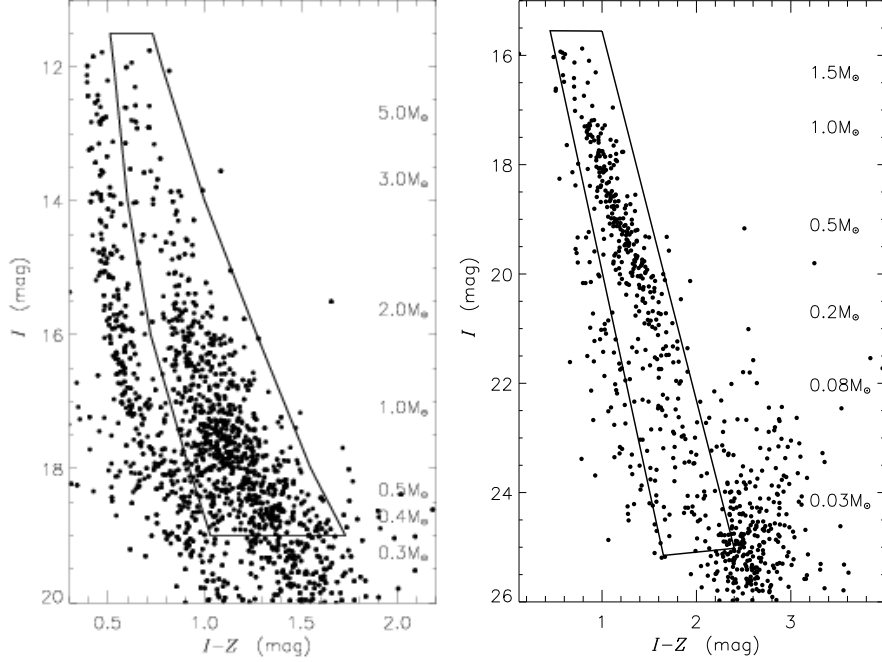


Figure 8. Left: Colour-magnitude diagram for the central $7 \text{ arcmin} \times 6 \text{ arcmin}$ region of NGC 6611 (Oliveira et al. 2005). The PMS can be clearly seen, separated from the bulk of field star contamination. Approximate PMS masses are indicated (Siess, Dufour & Forestini 2000) for a distance 1.8 kpc, an age of 3 Myr and $E(B - V) = 0.7 \text{ mag}$ (Sect. 3). Right: HST colour-magnitude diagram of the central 2.5 arcmin^2 area (Oliveira et al. 2008). Approximate PMS masses are indicated (Baraffe et al. 1998). The clump of red stars ($2 \lesssim I - Z \lesssim 3$) are evolved stars towards the Galactic Center. Note that the ground-based and HST filter sets are very different and no attempt was made to harmonize the magnitudes.

4.3 Low-mass Stars and Brown Dwarfs: IMF and Disk Population

Only recently has it become possible to probe the low-mass and brown dwarf populations of NGC 6611. Oliveira et al. (2005) performed an $I-Z$ survey of the cluster, with complementary JHK_L' imaging covering the central $4 \text{ arcmin} \times 5 \text{ arcmin}$ area. In the optical colour-magnitude diagram the rich low-mass PMS can easily be identified down to masses of $\sim 0.5 M_\odot$ (Fig. 8 left). Oliveira et al. (2008) used HST to extend the study of the PMS population to well below the substellar boundary, to about $0.02 M_\odot$ (Fig. 8 right). These observations add several hundreds of cluster candidates to the published samples, reaching for the first time into the brown dwarf regime.

Oliveira et al. (2008) constructed the IMF for the central 2.5 arcmin^2 region of NGC 6611 (Fig. 9) using the datasets described above. In agreement with published work described previously, for higher masses the slope of the IMF is consistent with a Salpeter index. For lower masses the IMF seems to flatten between $\sim 0.3 - 1 M_\odot$, with a peak at $\sim 0.4 - 0.5 M_\odot$, and then drop into the brown dwarf regime (slope $\Gamma \sim 0.7$), consistent with a power-law IMF as described by Kroupa (2001). The brown dwarf to

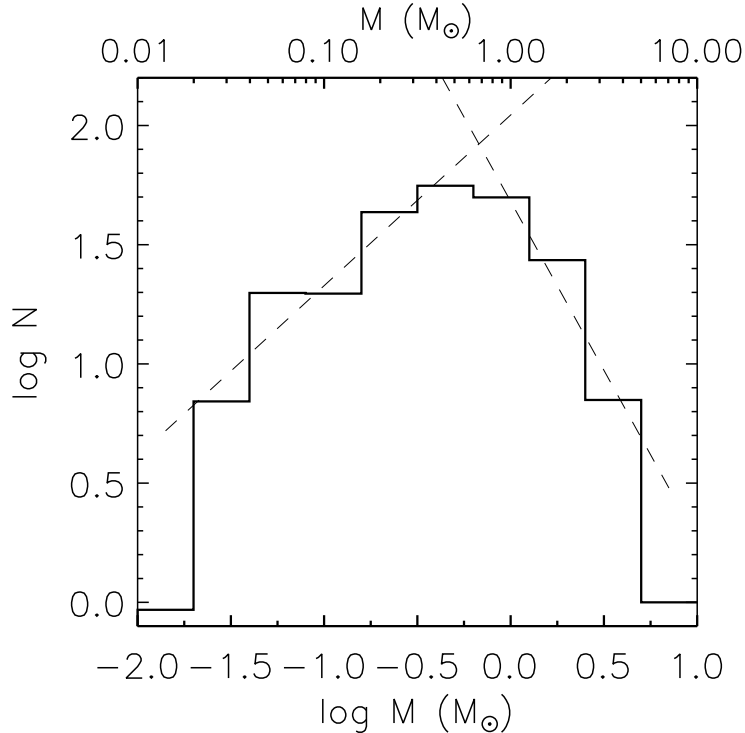


Figure 9. Initial Mass Function for the central region of NGC 6611 (Oliveira et al. 2008). Power-law IMF slopes of $\Gamma = -1.4$ and $\Gamma = 0.7$ are plotted for reference (Kroupa 2001).

star ratio of ~ 0.13 is consistent with other star forming regions (Luhman et al. 2003). For a full discussion of the IMF in NGC 6611 refer to Oliveira et al. (2008).

Near-IR photometry was used by Oliveira et al. (2005) to investigate the population of young low-mass stars that retain their circumstellar disks (i.e. CTTS). Circumstellar dust disks are commonly found around very young low-mass stars. If a young PMS star exhibits an IR colour in excess of the stellar photosphere this indicates the presence of a circumstellar disk. The cluster colour-colour diagrams are shown in Fig. 10: the *JHK* diagram diagnoses mainly massive accretion disks (e.g. Hillenbrand et al. 1998) while the *JHKL* diagram detects the large majority of circumstellar dusty disks at this young age (e.g. Haisch et al. 2001). Oliveira et al. (2005) found that the disk frequency in the inner area of NGC 6611 (50–60%) is consistent with similarly aged but quieter (i.e. with no O-stars) nearby star forming regions (Haisch, Lada & Lada 2001).

5 X-ray Emission in M 16

Guarcello et al. (2007) and Linsky et al. (2007) analyse the same Chandra X-ray Observatory images of NGC 6611; the ACIS-I detector with $16.9 \text{ arcsec} \times 16.9 \text{ arcsec}$ field-of-view covers a large fraction of M 16, including the HST-identified columns and the

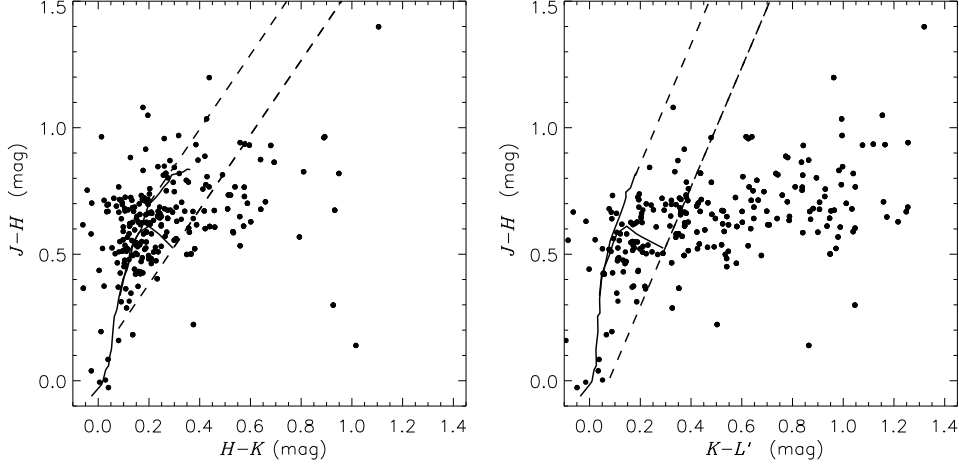


Figure 10. Intrinsic colour-colour diagrams for PMS objects in NGC 6611, JHK (left) and $JHKL'$ (right), from Oliveira et al. (2005). The loci of main-sequence and giant stars are represented (solid lines), as well as the reddening band (dashed lines). Objects to the right of the reddening band have an $H - K$ or $K - L'$ excess indicative of the presence of a dusty circumstellar disk.

denser cluster region of NGC 6611. Guarcello et al. (2007) use the X-ray catalogue combined with 2MASS K-band photometry to claim that there is a deficit of young stars with circumstellar disks (as indicated by a K-band excess) towards the cluster centre, possible evidence of the destructive power of the massive stars in the cluster. However, as discussed in the previous section, this method does not identify the majority of objects with circumstellar disks.

Linsky et al. (2007) have concentrated on the region associated with the dusty pillars. They find that the vast majority of X-ray sources in this region are moderately reddened young stars with small near-IR excesses. Only two hard X-ray sources are identified with embedded protostars near or within the dusty pillars — these sources are discussed in more detail in Section 7. None of the EGGs analysed by McCaughrean & Andersen (2002) have associated X-ray emission. Of the 11 EGGs with IR counterparts, 7 have substellar masses and thus are expected to be below the survey’s detection threshold. More unexpectedly, the 4 EGGs with masses $0.35\text{--}1.0 M_{\odot}$ are also not detected in the X-ray survey and Linsky et al. (2007) conclude that these EGGs do not emit X-rays at the level that one would expect for T Tauri stars. It is possible that these objects are at the very early stages of YSO evolution and have not yet become X-ray active. For the majority of the EGGs, however, both the lack of IR and X-ray associated sources seems to hint that many of the EGGs do not contain embedded YSOs.

6 Water Maser Emission in M 16

Water maser emission sources found in the molecular gas that surrounds H II regions are a clear indication of objects in the earliest stages of formation. Observational studies suggest that maser activity is associated with YSOs of all luminosities and it normally

lies in close proximity to the exciting object (e.g. Tofani et al. 1995; Furuya et al. 2001). Thus, water masers are powerful probes of embedded star formation, even if their intrinsic variability (Palagi et al. 1993; Tofani et al. 1995; Felli et al. 2007) means that not all embedded YSOs are uncovered by this type of observations.

Water maser emission in the Eagle Nebula was first identified by Yngvesson et al. (1975) and Blitz & Lada (1979) towards W 37. The nature of maser observations implies that surveys of complete star forming regions are normally impractical. Thus, one normally searches for maser emission in locations where star formation is suspected, for instance by the presence of embedded IR sources. As a result, several maser sources associated with IRAS sources were identified in M 16: IRAS 18156–1343 (Codella et al. 1994), IRAS 18152–1346 (Braz & Epchtein 1983; Codella et al. 1995) and IRAS 18159–1346 (associated with SFO 30, Braz & Epchtein 1983; Healy et al. 2004; Valdetarro et al. 2005) — Molinari et al. (1996) searched for ammonia towards IRAS 18156–1343 but no emission was detected. No maser emission was detected towards two other IRAS sources in the region, IRAS 18164–1340 and IRAS 18160–1339 (Szymczak, Hrynek & Kus 2000). All these sources are located in the dense region to the north of the massive stars in the cluster. Recent surveys have not detected maser emission towards W 37 as initially reported; this is probably due to the poorer spatial resolution of those early surveys and it is likely they detected the masing source associated with SFO 30 and IRAS 18159–1346.

Recently, Healy et al. (2004) performed several VLA pointings towards M 16, concentrating mainly on the dusty pillars. A total of 8 water masers were detected: a single component towards column II, one component in column IV likely associated with the driving source of HH 216 (Section 7.1), three components in column V and a further 3 components at the location of SFO 30 (Section 2.2). Typical separations between water masers and the YSOs that excite them are of the order of tens to hundreds of AU for low-mass protostars (e.g. Furuya et al. 2000) and $\lesssim 10^4$ AU for massive protostars (e.g. Tofani et al. 1995; Foster & Caswell 2000). For the locations with several maser detections, the physical separation between the components is at least 10^4 AU, implying that the masing activity is associated with multiple protostars. These observations further reinforce the notion that star formation is ongoing in several locations in the Eagle Nebula.

7 Individual Objects of Particular Interest

7.1 The Herbig-Haro Object HH 216

Herbig-Haro (HH) objects are optically bright, shock-excited nebulae powered by outflows from YSOs (see Reipurth & Bally 2001 for a review on HH objects) and thus also act as signposts for embedded star formation occurring nearby. The HH object in M 16 (see Figs. 3 and 11) was first identified by Meaburn & White (1982) near what is now known as column IV; initially labelled M16-HH1 it was later renamed HH 216 (Reipurth 1999). Several authors report optical and UV spectroscopic observations of this object (Meaburn 1982; Meaburn & Walsh 1984; Meaburn & Whitehead 1990).

Andersen et al. (2004) have identified what appears to be the counter bow shock to HH 216 (Fig 11), based on optical line emission, CO and CS emission, near-IR imaging and gas kinematics. While HH 216 is redshifted with a radial velocity of 150 km s^{-1} , the new emission-line object is blueshifted with a radial velocity of -150 km s^{-1} . A

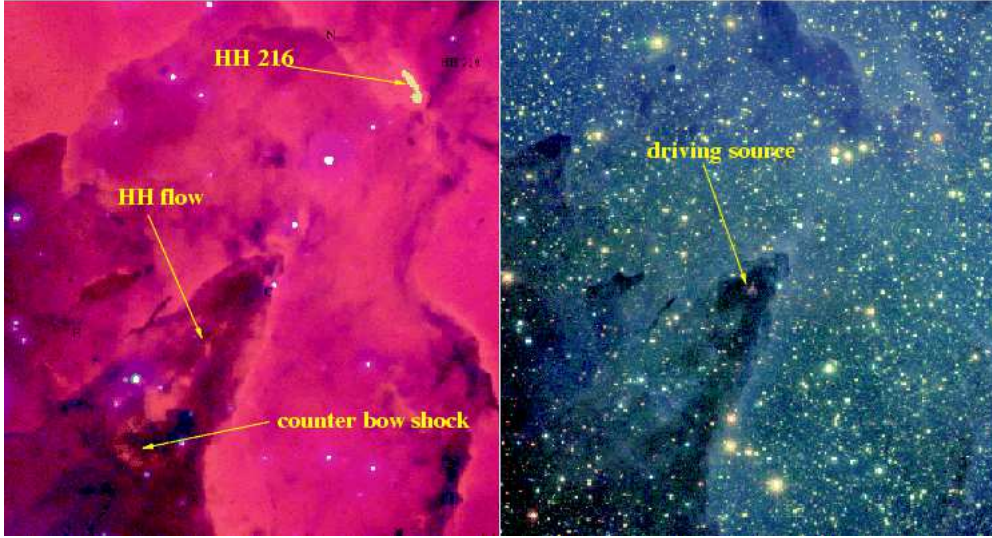


Figure 11. Colour composite images of HH 216 and column IV (Andersen et al. 2004). Left: $H\alpha$ (red), $[S\ II]$ (green) and continuum (blue); Right: true-colour JHK image. The optical composite shows the positions of HH 216, the counter bow shock and the HH flow. The IR composite shows the possible location of the driving source (see text).

string of optical or IR emission knots lies between these two objects. A small near-IR extended nebula, symmetrically placed between the two HH objects, points at the location of the embedded driving source of the HH system. Water maser emission has also been detected associated with this object (see previous section).

Linsky et al. (2007) found a weak X-ray source at the location of HH 216. This source has a mean photon energy of the order of 1.9 keV and an X-ray luminosity of $\sim 10^{30}$ erg s $^{-1}$, comparable to other HH objects. It is thought that X-ray emission in these objects originates from mechanical heating between the jet and the circumstellar medium (e.g. Bonito et al. 2004). No X-ray emission was detected towards the driving source of the HH 216 outflow.

7.2 Massive Embedded YSOs

The tips of columns I and II (Fig. 3) and column V (Fig. 4) show evidence of bright YSOs, first identified in IR images (Hillenbrand et al. 1993). The most recent analysis was performed by Indebetouw et al. (2007) who used Spitzer 3.6–24 μ m photometry to constrain the Spectral Energy Distribution (SED) of several YSOs. Some of those YSO sources have been subject to close scrutiny (Thompson et al. 2002; Sugitani et al. 2002; McCaughrean & Andersen 2002; Linsky et al. 2007; Sugitani et al. 2007; Indebetouw et al. 2007) and are here described in more detail.

YSO M16 ES-1: YSO M16 ES-1 (Thompson et al. 2002) is a very bright and red IR source at the tip of column I (YSO1 in McCaughrean & Andersen 2002; P1 in Sugitani et al. 2002). It was also detected at mid-IR wavelengths by MSX (Price et al. 2001) and ISO (Pilbratt et al. 1998). Thompson et al. (2002) integrated the object's

near-, mid- and far-IR fluxes to estimate a luminosity $L_{\text{bol}} \sim 200 L_{\odot}$, indicative of a $4\text{--}5 M_{\odot}$ ZAMS star. Assuming that the observed J and H magnitudes are photospheric, McCaughrean & Andersen (2002) find that these fluxes are consistent with a deeply embedded ($A_V \sim 27$ mag), $10 M_{\odot}$ ZAMS star. However, Thompson et al. (2002) find no $\text{Pa}\alpha$ emission at the location of this source, suggesting that it cannot be a single ZAMS object (not even a late B spectral type object). Thus, this object could either be a small cluster of low-mass PMS stars or an early protostellar source. Its large IR excess (McCaughrean & Andersen 2002) suggests an embedded YSO. Fukuda et al. (2002) report the presence of 2.7 mm continuum emission at the position of ES-1 that they suggest is due to dust emission, even though it could also be free-free emission from an ultracompact H II region.

Sugitani et al. (2007) identifies strong polarized emission (in the H- and K-bands) asymmetrically distributed north and south of ES-1. They suggest this emission originates from the walls of two cavity lobes, which were created by the molecular outflow from the central object. A clear gap in polarization intensity is seen between the two lobes, that they propose corresponds to a disk-like structure (previously suggested by Sugitani et al. 2002), perpendicular to the axis of the cavity lobes. Furthermore, the disk appears to be tilted so that higher polarization intensity is produced at the north lobe, while higher degree of polarization is detected at the south lobe.

Linsky et al. (2007) identify ES-1 with a very bright and hard X-ray source. They estimate $L_X \sim 1.6 \times 10^{32} \text{ erg s}^{-1}$, $L_X/L_{\text{bol}} \sim 2.1 \times 10^{-4}$, mean photon energy $\bar{e} = 3.3 \text{ keV}$ and plasma temperature of $\sim 2.2 \text{ keV}$. These properties are consistent with those observed for other young, magnetic O-stars (heating by magnetically channelled wind shocks), but very different from typical O-stars with X-ray emission produced in weak shocks. Thus they conclude that ES-1 is most likely a magnetically active, high-mass YSO.

Indebetouw et al. (2007) analysed Spitzer photometry for ES-1. The $2\text{--}24 \mu\text{m}$ spectral index and mass accretion rate ($1 - 70 \times 10^{-5} M_{\odot} \text{ yr}^{-1}$) are consistent with a Class I source. These authors estimate a bolometric luminosity of $44 \pm 10 L_{\odot}$. Using fits to the object's SED, they estimate a mass of $4.5 M_{\odot}$, with a total extinction (foreground and circumstellar) of $A_V \sim 40$ mag.

YSO M16 ES-2: YSO M16 ES-2 (Thompson et al. 2002) sits at the tip of column II (YSO2 in McCaughrean & Andersen 2002; T1 in Sugitani et al. 2002). Compared to ES-1, this source is less luminous ($L_{\text{bol}} \sim 20 L_{\odot}$, Thompson et al. 2002; Indebetouw et al. 2007) and less obscured ($A_V \sim 15$ mag, McCaughrean & Andersen 2002), with an estimated mass of $2\text{--}5 M_{\odot}$ (Thompson et al. 2002; McCaughrean & Andersen 2002; Indebetouw et al. 2007). Based on its near-IR excess (Sugitani et al. 2002) and mid-IR spectral index (Indebetouw et al. 2007), ES-2 has been classified as a Class II object, i.e., probably at a more evolved stage than ES-1. Water maser emission detected at the tip of column II is not associated with ES-2 (Healy et al. 2004). Similarly to ES-1, Sugitani et al. (2007) detect polarized emission at the position of ES-2 and propose the presence of a tilted disk-like structure around this object.

ES-2 is the weakest of the X-ray sources considered by Linsky et al. (2007). They estimate $L_X \sim 1.26 \times 10^{30} \text{ erg s}^{-1}$ and $L_X/L_{\text{bol}} \sim 1.6 \times 10^{-5}$. They note that the X-ray luminosity of ES-2 is consistent with similar mass young objects in Orion, but the luminosity ratio is rather low. However, these estimates are very uncertain due to the small number of detected counts (5 raw counts). Still, it is possible that this object is

too young to be significantly X-ray active, similarly to the 4 massive EGGs mentioned in Section 5.

Massive YSOs in Column V: Indebetouw et al. (2007) has constructed the SEDs of 2 embedded sources located in column V. P5 A is located at the tip of this column and it is marginally resolved in the Spitzer images, with two IR components corresponding to two of the three masing sources identified by Healy et al. (2004). This source has a high spectral index, a luminosity of $\sim 250 L_{\odot}$ and it is very bright at $24\mu\text{m}$, consistent with it being a young intermediate mass ($\sim 6 M_{\odot}$) YSO. The object identified as P5 B sits at the base of the column; it is less luminous ($\sim 200 L_{\odot}$) than P5 A but it is also likely to be an embedded YSO.

IRAS 18152–1346: IRAS 18152–1346 is the most luminous YSO identified so far in M 16 and is located to the west of the main pillars, in a little studied region. This IR source is also associated with water maser emission (Braz & Epchtein 1983; Codella et al. 1995). Fits to the SED suggest that this object has a luminosity of $\sim 1000 L_{\odot}$ and a mass of $8 M_{\odot}$ (Indebetouw et al. 2007).

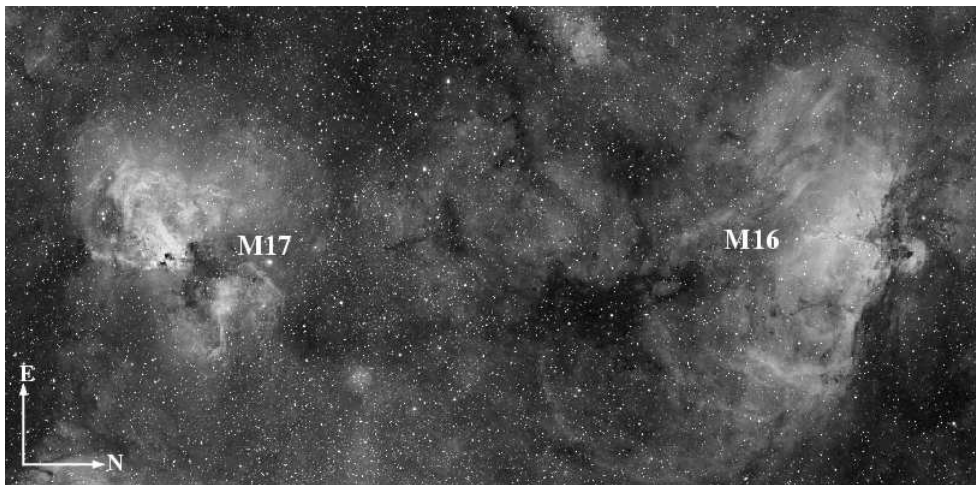


Figure 12. M 16 and M 17 might be part of the same star-forming cloud complex in the Sagittarius arm ($H\alpha$ image courtesy of Russell Croman).

8 A Link between M 16 and M 17

Both M 16 and M 17 (the Omega Nebula) are large star forming regions in the Sagittarius spiral arm (Georgelin & Georgelin 1970), at distances from the Sun of 2.1 kpc for M 17 (see chapter by Chini & Hoffmeister) and 1.8 kpc for M 16. Their angular separation is about 2.5° (Fig. 12).

Based on ^{12}CO emission maps Elmegreen, Lada & Dickinson (1979) show that there is tenuous molecular material connecting M 16 and M 17 and region III (a complex located to the southwest of M 17). This suggests that the whole region is a quasi-continuous molecular structure, within which these massive individual clouds have con-

densed and begun to form stars (see also Moriguchi et al. 2002). Sofue et al. (1986) further propose that NGC 6604 (located to the north of NGC 6611) is also part of this “long string of beads” of star forming activity along the Sagittarius arm. They suggest that it also defines an age sequence: the older region NGC 6604 (age ~ 4 Myr, see chapter by Reipurth) triggers star formation in M 16 (age $\sim 2 - 3$ Myr), then M 17 (age ~ 1 Myr), via stellar-wind or supernova-blown bubbles. Alternatively, these regions are a natural progression of star formation as molecular clouds collapse and form stars due to the passage of the spiral arm.

These regions might actually be part of an even larger star formation complex (Stal’bovskii & Shevchenko 1981) that includes also M 8 (the Lagoon Nebula) and M 20 (the Trifid Nebula), extending along the Sagittarius arm at $l = 13^\circ \pm 4^\circ$. The location and typical scales of this super-star forming region in the spiral arms of our Galaxy are consistent with what is observed in other spiral galaxies, offering us a route to understand the mechanisms for star formation at large (galactic) scales in the Milky Way.

Acknowledgements. JMO acknowledge financial support from the UK Science and Technology Facilities Council. I would like to thank all authors that have contributed with figures to this manuscript.

References

- Alecian, E., Wade, G.A., Catala, C. et al., 2008, *A&A*, 481, L99
 Allen, L.E., Burton, M.G., Ryder, S.D., Ashley, M.C.B., & Storey, J.W.V, 1999, *MNRAS*, 304, 98
 Andersen, M., Knude, J., Reipurth, B. et al., 2004, *A&A*, 414, 969
 Anglada, G., Estalella, R., Pastor, J., Rodriguez, L.F., & Haschick, A.D., 1996, *ApJ*, 463, 205
 Baumgardt, H., Dettbarn, C., & Wielen, R., 2000, *A&AS*, 146, 251
 Baraffe, I., Chabrier, G., Allard, F., Hauschildt, P., 1998, *A&A*, 337, 403
 Becker, W., 1963, *Zeitschrift f. Astrophysik*, 57, 117
 Beech, M. & Mitalas, R., 1994, *ApJS*, 95, 517
 Belikov, A.N., Kharchenko, N.V., Piskunov, A.E., & Schilbach, E., 1999, *A&AS*, 134, 525
 Belikov, A.N., Kharchenko, N.V., Piskunov, A.E., & Schilbach, E., 2000, *A&A*, 358, 886
 Blitz, L. & Lada, C.J., 1979, *ApJ*, 227, 152
 Bonatto, C., Santos Jr., J.F.C., & Bica, E., 2006, *A&A*, 445, 567,
 Bonito, R., Orlando, S., Peres, G., Favata, F., & Rosner, R., 2004, *A&A*, 424, 1
 Bonnell, I.A., Bate, M.R., & Zinnecker, H., 1998, *MNRAS*, 298, 93
 Bosch, G.L., Morrell, N.I., & Niemelä, V.S., 1999, *RMxAA*, 35, 85
 Braz, M.A. & Epchtein, N., 1983, *A&AS*, 54, 167
 Brown, P.J.F., Dufton, P.L., Lennon, D.J., Keenan F.P., & Kilkenny D., 1986, *A&A*, 155, 113
 Chini, R. & Krügel, E., 1983, *A&A*, 117, 289
 Chini, R. & Wargau, W.F., 1990, *A&A*, 227, 213
 Chini, R., Krügel, E., & Wargau, W.F., 1992, *A&A*, 265, 45
 Codella, C., Felli, M., Natale, V., Palagi, F., & Palla, F., 1994, *A&A*, 291, 261
 Codella, C., Palumbo, G.G.C., Pareschi, G. et al., 1995, *MNRAS*, 276, 57
 Cutri, R.M., Skrutskie, M.F., van Dyk, S. et al., 2003, *The IRSA 2MASS All-Sky Point Source Catalog*, NASA/IPAC Infrared Science Archive, <http://irsa.ipac.caltech.edu>
 Daflon, S., Cunha, K., & Butler, K., 2004, *ApJ*, 604, 362
 de Winter, D., Koulis, C., Thé, P.S. et al., 1997, *A&AS*, 121, 223
 Dieter, N.H., 1967, *ApJ*, 150, 435
 Duchêne, G., Simon, T., Eisloffel, J., & Bouvier J., 2001, *A&A*, 379, 147
 Dufton, P.L., Smartt, S.J., Lee, J.K. et al., 2006, *A&A*, 457, 265

- Duncan, J.C., 1920, ApJ, 51, 4
- Elliot, K.H., Meaburn, J., & Terrett, D.L., 1978, A&A, 70, 241
- Elmegreen, B.G., Lada, C.J., & Dickinson, D.F., 1979, ApJ, 230, 415
- Egan, M.P., Price, S.D., Kraemer, K.E. et al., 2003, *VizieR On-line Data Catalog: V/114*. Originally published in: Air Force Research Laboratory Technical Report AFRL-VS-TR-2003-1589
- Evans, C.J., Smartt, S.J., Lee, J.-K. et al., 2005, A&A, 437, 467
- Felli, M. & Churchwell, E., 1970, ApJ, 160, 43
- Felli, M., Testi, L., Schuller, F., & Omont, A., 2002, A&A, 392, 971
- Felli, M., Brand, J., Cesaroni, R. et al., 2007, A&A, 476, 373
- Foster, J.R. & Caswell, J.L., 2000, ApJ, 530, 371
- Fukuda, N., Hanawa, T., & Sugitani, K., 2002, ApJ, 568, 127
- Furuya, R.S., Kitamura, Y., Wootten, H.A. et al., 2000, ApJ, 542, 135
- Furuya, R.S., Kitamura, Y., Wootten, H.A., Claussen, M.J., & Kawabe, R., 2001, ApJ, 559, 143
- García-Rojas, J., Esteban, C., Peimbert, M. et al., 2006, MNRAS, 368, 253
- Georgelin, Y.P. & Georgelin, Y.M., 1970, A&A, 6, 349
- Gebel, W.L., 1968, ApJ, 153, 743
- Goudis, C., 1975, Ap&SS, 38, 13
- Goudis, C., 1976, Ap&SS, 41, 105
- Goudis, C. & Meaburn, J., 1976, A&A, 51, 401
- Guarcello, M.G., Prisinzano, L., Micela, G. et al., 2007, A&A, 462, 245
- Guenther, E.W. & Emerson, J.P., 1997, A&A, 321, 803
- Gum, C.S., 1955, MmRAS, 67, 155,
- Haisch, K.E. Jr., Lada, E.A., Piña, R.K. et al., 2001, AJ, 121, 1512
- Haisch, K.E. Jr., Lada, E.A., & Lada, C.J., 2001, ApJ, 553, 153
- Healy, K.R., Hester, J.J., & Claussen, M.J., 2004, ApJ, 610, 835
- Hébrard, G., Péquignot, D., Walsh, J.R., Vidal-Madjar, A., & Ferlet, R., 2000, A&A, 364, 31
- Herbig, G.H. & Dahm, S.E., 2001, PASP, 113, 195
- Hester, J.J., Scowen, P.A., Sankrit, R. et al., 1996, AJ, 111, 2349
- Hester, J.J. & Desch, S.J., 2005, in *Chondrites and the Protoplanetary Disk*, ASP Conference Series Vol. 341, eds. A. Krot, E. Scott & B. Reipurth, p. 107
- Hillenbrand, L.A., Strom, S.E., Calvet, N. et al., 1998, AJ, 116, 1816
- Hillenbrand, L.A., Massey, P., Strom, S.E., & Merrill, K.M., 1993, AJ, 106, 1906
- Hiltner, W.A. & Morgan, W.W., 1969, AJ, 74, 1152
- Hoag, A.A., Johnson, H.L., Iriarte, B. et al., 1961, PUSNO, 17, 345
- Indebetouw, R., Robitaille, T.P., Whitney, B.A. et al., 2007, ApJ, 666, 321
- Johnson, H.M., 1973, PASP, 85, 586
- Kamp, L.W., 1974, A&AS, 16, 1
- Kharchenko, N. & Schilbach, E., 1995, AN, 316, 91
- Kharchenko, N.V., Piskunov, A.E., Roeser, S., Schilbach, E., & Scholz, R.-D., 2005, A&A, 438, 1163
- Kroupa, P., 2001, MNRAS, 322, 231
- Kumar, B., Sagar, R., Sanwal, B.B., & Bessell, M.S., 2004, MNRAS, 353, 991
- Levenson, N.A., Graham, J.R., McLean, I.S. et al., 2000, ApJ, 533, 53
- Linsky, J.L., Gagné, M., Mytyk, A., McCaughrean, M., & Andersen, M., 2007, ApJ, 654, 347
- Loktin, A.V. & Beshenov, G.V., 2003, Astron. Zh., 80, 8
- Luhman, K.L., Stauffer, J.R., Muench, A.A. et al., 2003, ApJ, 593, 1093
- Massey, P., Johnson, K.E., & DeGioia-Eastwood, K., 1995, ApJ, 454, 151
- McBreen, B., Fazio, G.G., & Jaffe, D.T., 1982, ApJ, 254, 126
- McCaughrean, M.J. & Andersen, M., 2002, A&A, 389, 513
- Meaburn, J., 1982, A&A, 114, 367
- Meaburn, J. & White, N.J., 1982, MNRAS, 199, 121
- Meaburn, J. & Walsh, J.R., 1984, A&A, 138, 36
- Meaburn, J. & Walsh, J.R., 1986, MNRAS, 220, 745
- Meaburn, J. & Whitehead, M.J., 1990, A&A, 235, 395

- Mezger, P.G. & Höglund, B., 1967, ApJ, 147, 490
- Miao, J., White, G.J., Nelson, R., Thompson, M., & Morgan, L., 2006, MNRAS, 369, 143
- Miller, J.S., 1968, ApJ, 151, 473
- Mizuta, A., Kane, J.O., Pound, M.W. et al., 2006, ApJ, 647, 1151
- Molinari, S., Brand, J., Cesaroni, R., & Palla, F., 1996, A&A, 308, 573
- Morgan, L.K., Thompson, M.A., Urquhart, J.S., & White, G.J., 2008, A&A, 477, 557
- Morgan, L.K., Thompson, M.A., Urquhart, J.S., White, G.J., & Miao, J., 2004, A&A, 426, 535
- Moriguchi, Y., Onishi, O., Mizuno, A., & Fukui, Y., 2002, in the *Proceedings of the IAU 8th Asian-Pacific Regional Meeting*, Volume II, Tokyo, eds. S. Ikeuchi, J. Hearnshaw & T. Hanawa, PASJ, p. 173
- Mufson, S.L., Fountain, W.F., Gary, G.A. et al., 1981, ApJ, 248, 992
- Neckel, T. & Chini, R., 1981, A&AS, 45, 451
- Ogura, K., Sugitani, K., & Pickles, A., 2002, AJ, 123, 2597
- Oliveira, J.M., Jeffries, R.D., van Loon, J.Th., Littlefair, S.P., & Naylor, T., 2005, MNRAS, 358, L 21
- Oliveira, J.M., Jeffries, R.D., van Loon, J.Th., 2008, MNRAS, submitted
- Orsatti, A.M., Vega, E.I., & Marraco, H.G., 2000, A&AS, 144, 195
- Orsatti, A.M., Vega, E.I., & Marraco, H.G., 2006, AJ, 132, 1783
- Palagi, F., Cesaroni, R., Comoretto, G., Felli, M., & Natale, V., 1993, A&AS, 101, 153
- Palla, F. & Stahler, S.W., 1993, ApJ, 418, 414
- Paunzen, E., Pintado, O.I., & Maitzen, H.M., 2002, A&A, 395, 823
- Pandey, A.K., Mahra, H.S., & Sagar, R., 1992, BASI, 20, 287
- Pilbratt, G.L., Altieri, B., Blommaert, J.A.D.L., Fridlund, C.V.M., Tauber, J.A., & Kessler, M.F., 1998, A&A, 333, 9
- Pound, M.W., 1998, ApJ, 493, 113
- Price, S.D., Egan, M.P., Carey, S.J., Mizuno, D.R., & Kuchar, T.A., 2001, AJ, 211, 2819
- Quireza, C., Rood, R.T., Balser, D.S., & Bania, T.M., 2006, ApJS, 165, 338
- Reipurth, B., 1999, *A general catalogue of Herbig-Haro objects*, 2nd edition, <http://casa.colorado.edu/hhcat>
- Reipurth, B. & Bally, J., 2001, ARA&A, 39, 403
- Rodgers, A.W., Campbell, C.T., & Whiteoak, J.B., 1960, MNRAS, 121, 103
- Sagar, R. & Joshi, U.C., 1979, Ap&SS, 66, 3
- Scalo, J.M., 1986, Fundam. Cosmic Phys., 11, 1
- Schaller, G., Schaerer, D., Meynet, G., & Maeder, A., 1992, A&AS, 96, 269
- Schmidt-Kaler, Th., 1982, *Landolt-Börnstein Numerical Data and Functional Relationships in Science and Technology*, New Series, Group IV, Springer-Verlag Press, Berlin-Heidelberg, New York, 2, p. 15
- Schuller, F., Leurini, S., Hieret, C. et al., 2006, A&A, 454, 87
- Sharpless, S., 1959, ApJS, 4, 257
- Siess, L., Dufour, E., & Forestini, M., 2000, A&A, 358, 593
- Sofue, Y., Handa, T., Fürst, E., Reich, W., & Reich, P., 1986, PASJ, 38, 257
- Stal'bovskii, O.I. & Shevchenko, V.S., 1981, SvA, 25, 25
- Sugitani, K., Fukui, Y., & Ogura, K., 1991, ApJS, 77, 59
- Sugitani, K., Tamura, M., & Nakajima, Y., 2002, ApJ, 565, 25
- Sugitani, K., Watanabe, M., Tamura, M. et al., 2007, PASJ, 59, 481
- Szymczak, M., Hrynek, G., & Kus, A.J., 2000, A&AS, 143, 269
- Thé, P.S., de Winter, D., Feinstein, A., & Westerlund, B.E., 1990, A&AS, 82, 319
- Thompson, R.I., Smith, B.A., & Hester, J.J., 2002, ApJ, 570, 749
- Tofani, G., Felli, M., Taylor, G.B., & Hunter, T.R., 1995, A&AS, 112, 299
- Tucholke, H.-J., Geffert, M., & Thé, P.S., 1986, A&AS, 66, 311
- Urquhart, J.S., White, G.J., Pilbratt, G.L., & Fridlund, C.V.M., 2003, A&A, 409, 193
- Valdettaro, R., Palla, F., Brand, J., & Cesaroni, R., 2005, A&A, 443, 535
- van Schewick, H., 1962, Veröff. Univ. Sternw. Bonn 62, 1
- Walker, M.F., 1961, ApJ, 133, 438
- Walsh, J.R. & White, N.J., 1982, MNRAS, 199, 9

- Weidner, C. & Kroupa, P., 2006, MNRAS, 365, 1333
Westerhout, G., 1958, BAN, 14, 215
White, G.J., Nelson, R.P., Holland, W.S. et al., 1999, A&A, 342, 233
White, R.J. & Basri, G., 2003, ApJ, 582, 1109
Williams, R.J.R., Ward-Thompson, D., & Whitworth, A.P., 2001, MNRAS, 327, 788
Wolff, S.C., Strom, S.E., Dror, D., & Venn, K., 2007, AJ, 133, 1092
Yadav, R.K.S. & Sagar, R., 2001, MNRAS, 328, 370
Yngvesson, K.S., Cardenas, A.G., Shanley, J.F., Ellder, J., & Rydbeck, O.E.H., 1975, ApJ, 195, 91